Optimal hydrodynamic synchronization of colloidal rotors

Supplementary material

Introduction

The first section of this document describes in detail the different checks we have done on our data and provides an explanation of the lower strength of synchronization observed in the experiments. An empirical correction to the radial stiffness k_r, adjusting it by a multiplicative coefficient given in the main text, was found to account for what is likely a mix of the physical and instrumental factors described here. The second section provides the derivation of the strength of synchronization Γ (Eq. 3 in the main text).

1 Experimental considerations

1.1 Calibration of the force profile

In an experiment, the force profile $F(\phi)$ is measured for a given parameter A_2 on a single rotor. The measured profile is then used to redefine new distances between the bead and the trap for each point of the path that will match the desired profile. Calibrated profiles are shown in Fig. S1 and are very close to the expected profiles. Forces are calculated by measuring the average velocity of the particle depending on the angle ϕ on the path.

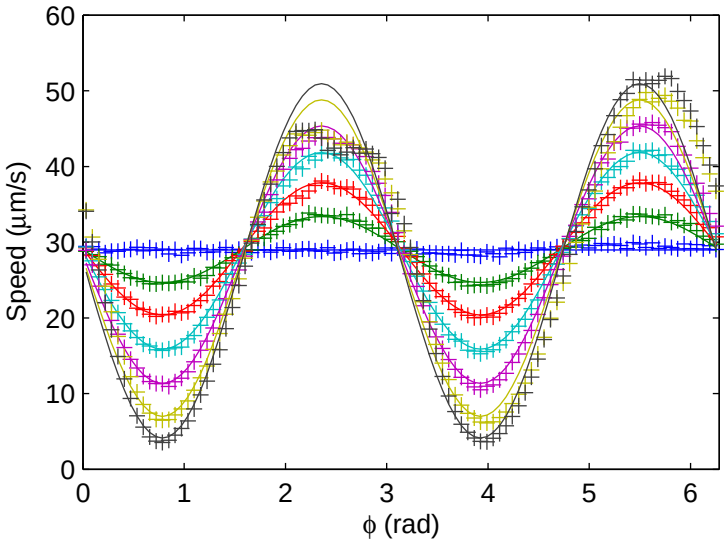

Supplementary Figure S1: Calibrated force profiles measured on a single rotor. Through calibration, a desired force profile can be implemented very accurately. Experiments (markers) and expected profiles (lines) for A_2 = 0, 0.15, 0.3, 0.45, 0.6, 0.75 and 0.85. For high A_2 it can be seen that the force saturates a little for some angles, i.e. it is not possible to move any faster.

1.2 Measure of the radial stiffness

1.2.1 Trapping in the radial direction

In the radial direction, the driving trap of a rotor is made of a line of 21 harmonic traps (with same intensity) that are scanned at 20 kHz. In the case of two rotors, the 21 traps of the first rotor are scanned, then the 21 traps of the other, etc. The separation between two traps is set between 0 and 0.2 μm in order to tune the radial trapping constant k_r. The size of the line segment is therefore varied between 0 and 4.4 μm. The trapping in the radial direction is not strictly harmonic over a wide range, but can be approximated by a harmonic trap for small fluctuations of the radius (see section 1.2.2).

1.2.2 Measure of the radial stiffness

The radial stiffness is measured for 50 different angles ϕ on a single-rotor movie. For each angle, it is defined as

$$k_r(\phi) = \frac{k_B T}{\mathrm{var}(r)}, \tag{S1}$$

with $\mathrm{var}(r)$ the variance of the radius for the given angle ϕ. The radial stiffness input in the theoretical formula is the average of $k_r(\phi)$ over all angles. The radial stiffness cannot be measured by taking the standard deviation of the radial fluctuations at all angles, because the radius of the trajectory is not perfectly constant (about 0.2 μm standard deviation, which is bigger than the standard deviation due to thermal fluctuations).

Fig. S2 shows distributions of r for four different angles. First, all these distributions look like Gaussians, so that the trap can be described by a harmonic potential in the range of thermal fluctuations. Second, although the average value varies with the angle, the standard deviation remains fairly constant, at least for small A_2. This is also shown for more angles in the plot of $k_r(\phi)$ (Fig. S3).

k_r is measured by looking at the thermal fluctuations along the radial direction. The displacements

are of the order of

$$\delta r^{\mathrm{therm}} \sim \sqrt{\frac{k_B T}{k_r}}. \tag{S2}$$

However, in the 2-rotors experiment, the fluctuations of the radial position of a particle due to the interaction with the other particle has a magnitude

$$\delta r^{\mathrm{coupl}} \sim \frac{a}{d} \frac{6\pi\eta a}{k_r}. \tag{S3}$$

With usual values of the parameters, we obtain $\delta r^{\mathrm{therm}} \sim 0.04$ μm and $\delta r^{\mathrm{coupl}} \sim 0.1$ μm. Therefore, thermal fluctuations do not probe a range of positions wide enough to claim that the potential is harmonic. However, measures of the anharmonicity of the potential of a single trap far from the centre showed that at a distance of 1 μm from the centre, the measured trapping force only differs by 30 % compared to the value calculated by using the trap constant k_r measured from thermal fluctuations. Therefore, it is likely to be correct to approximate the radial potential as harmonic in the relevant range $\delta r^{\mathrm{coupl}}$ of fluctuations of the radial position.

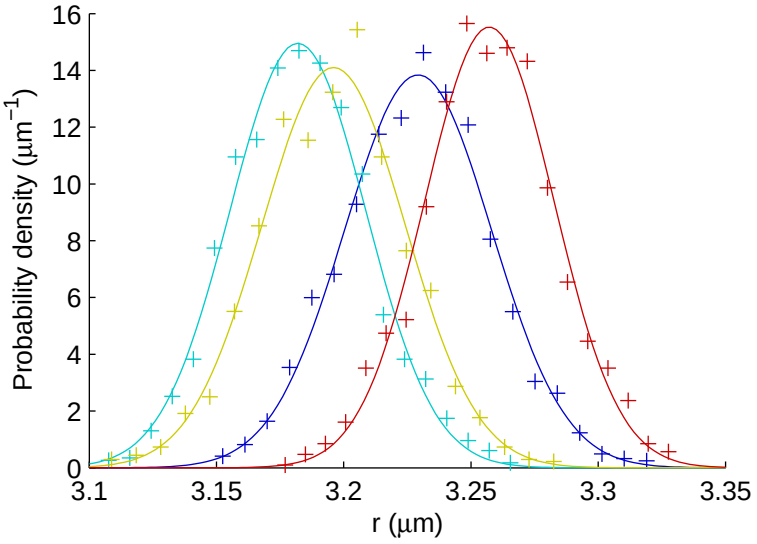

Supplementary Figure S2: Distribution of the radial position of a single rotor for four different angles: 0 (blue), $\pi/2$ (cyan), π (yellow) and $3\pi/2$ (red). The Gaussian fits (lines) match the experimental data (+) very well. The fitting parameters give values of k_r in agreement with the method used in the main text, in which we simply measured the standard deviation of the radius.

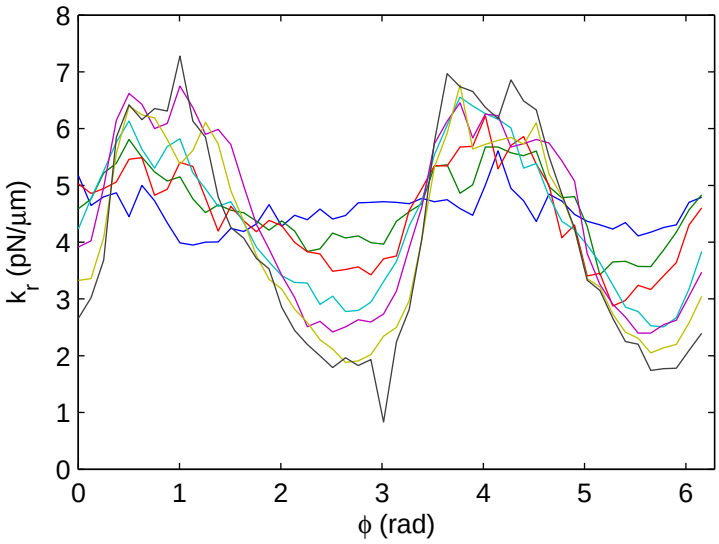

Supplementary Figure S3: Radial stiffness, measured as a function of the angle for a single rotor for different values of A_2. A_2 is changed as indicated in Fig. S1. For small A_2, the radial stiffness is fairly flat.

1.3 Detuning between the two oscillators

Since the coupling between the two rotors is quite small ($3a/(4d) < 0.1$, see section 1.8), the system is not strongly synchronized and the relaxation time is highly sensitive to a detuning in the intrinsic periods of each oscillator. The system is corrected for possible detunings by slightly increasing or decreasing the average (over all angles) of the trap-bead distance ϵ of one of the oscillators. Since the synchronized state is expected to be in phase, the detuning is adjusted such that the mean phase difference $\langle \Delta\phi \rangle$ between the two rotors is close to 0. Experimentally, the system was considered as not detuned when $\langle \Delta\phi \rangle$ was in the $[-0.1, 0.1]$ rad range.

Figures S4 and S5 show an experiment and the corresponding simulation in which detuning was deliberately introduced.

To remain synchronized in presence of detuning, the system adjusts its phase difference (Fig. S4). A mean phase difference of 0 should correspond to no detuning. The mean phase difference appears to moves in a wider range in the experiments than in the simulations, for a given range of detuning.

Fig. S5 shows that the detuning has a strong effect on the relaxation time. The experimental and simulated curves have a similar shape, but experiments are shifted towards a higher relaxation time. A portion of the shift can be explained by the interaction with the wall (see section 1.8). But there is also the possibility that the detuning is fluctuating over the duration (10 min) of an experiment. While the mean phase difference can still be set to zero, it only makes the average detuning equal to zero. Fluctuations of the detuning lead to less synchronization, and simulations in Fig. S5 suggest that it can account for a big part of the discrepancy.

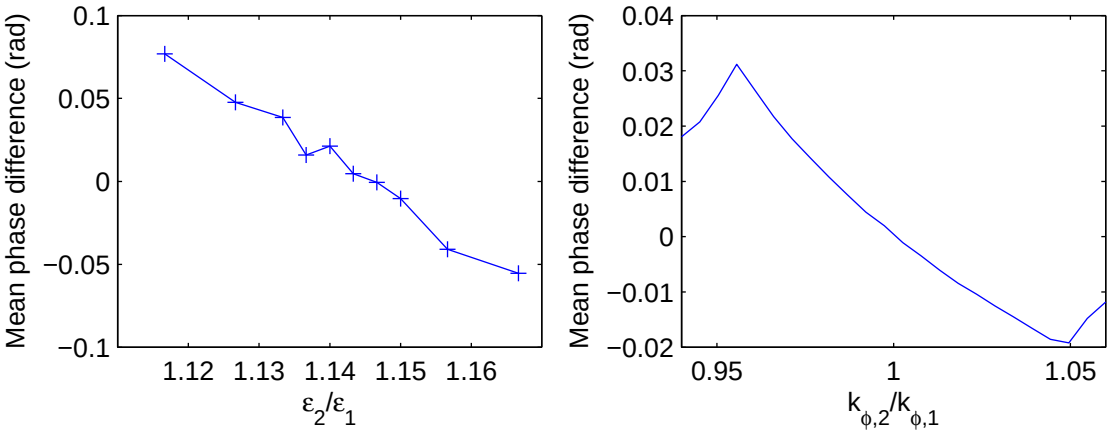

Supplementary Figure S4: Experiment (left) and simulation (right): Mean phase difference between the two oscillators depending on the detuning. In the experiments, detuning is controlled by changing the bead-trap distance ϵ_2 of the second oscillator, while in the simulation, we change the tangential trap stiffness $k_{\phi,2}$. In the experiments, the system is not detuned (in average) when ϵ_2/ϵ_1 is about 1.14.

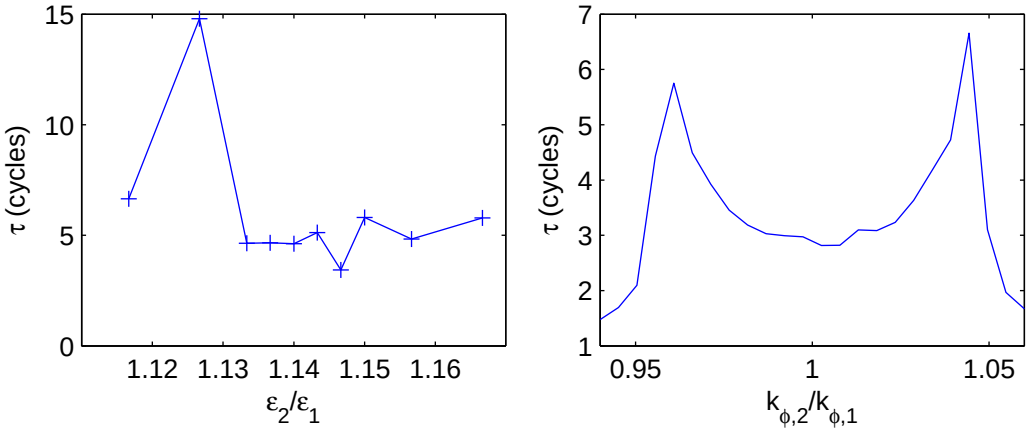

Supplementary Figure S5: Experiment (left) and simulation (right): Relaxation time depending on the detuning as explained in Fig. S4. One experimental point seems to be anomalous. Note that the range of detuning explored in the experiments is smaller than the one in the simulations. In the simulations, the sharp decreases in τ at extreme detuning correspond to a loss of synchronization. The expected relaxation time in the absence of detuning is about 3 cycles.

1.4 Feedback time: sampling and delay

In the Cambridge experimental setup (i.e. the experimental data in the main text figures, except Fig 2 inset), a computer analyzes frames at a rate of 229 fps, and updates the position of the traps lines at the same frequency. The feedback loop involves the time corresponding to this sampling frequency, but also any delay in the transmission of the images to the computer, and from the computer to the laser beam steering electronics. The total delay between the time at which a picture of the beads is taken and the time at which the traps are moved is 6.5 ± 0.1 ms (measurement on a single 1 min long movie).

This overall feedback time has an effect on the synchronization strength. The main time interval (i.e. the largest delay) occurs when the computer decides to move a trap: a command is sent to the AODs, but this is carried through the USB port which can have a latency time of up to 10 ms. It is under

control of the operating system, and is difficult to reduce even in the Linux system patched for real-time operation. Once the command has been transmitted, the traps are moved essentially instantaneously by the electronics controlling the AODs.

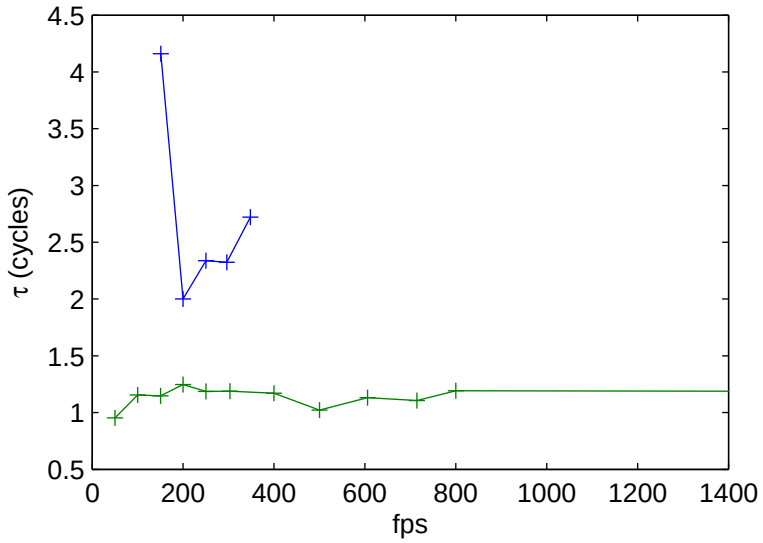

Supplementary Figure S6: Strength of synchronization depending on the sampling (feedback) frequency. Experiments in blue and simulations in green. From this analysis, looking at both experiments and simulations, it was concluded that a sampling frequency greater than 200 fps was adequate.

We explore first the effect of the sampling time (corresponding to the feedback frequency). The experiment in Fig. S6 shows that increasing the sampling frequency from 200 frames per second (fps) to higher values does not change significantly the strength of synchronization. Simulations also support this conclusion.

In a second set of simulations, we made the sampling frequency extremely fast, but included a delay in the motion of the traps. This delay appears to have a large effect on the strength of synchronization (figures S7 and S8). Even small delays of about 1/100 of a cycle increase dramatically the relaxation time, and move it towards the experimental points. However, a delay of the order of the one measured in the experiments ($\sim$6.5 ms) is not sufficient to explain by itself the shift between experimental and simulated curves.

1.5 Freedom along rotational axes

In the simulations and theory, the model for hydrodynamic interactions assumes point-like particles and a coupling described by a 2d Oseen tensor in the (x, y) plane. In the experiments, it might be possible that the particles rotate. However, if we assume that the tweezers are only applying translational forces, this does not induce any rotation of the particles [1].

1.6 Relaxation time of the trap along the radial direction

There is a relaxation time $6\pi\eta a/k_r$ linked to the radial stiffness. If this relaxation time is longer or of the same magnitude as the period of oscillation of a rotor, it could play a role in the state of synchronization. By using usual values for all the parameters, we find a "radial" relaxation time of 0.04 cycles, well below the period of the oscillators.

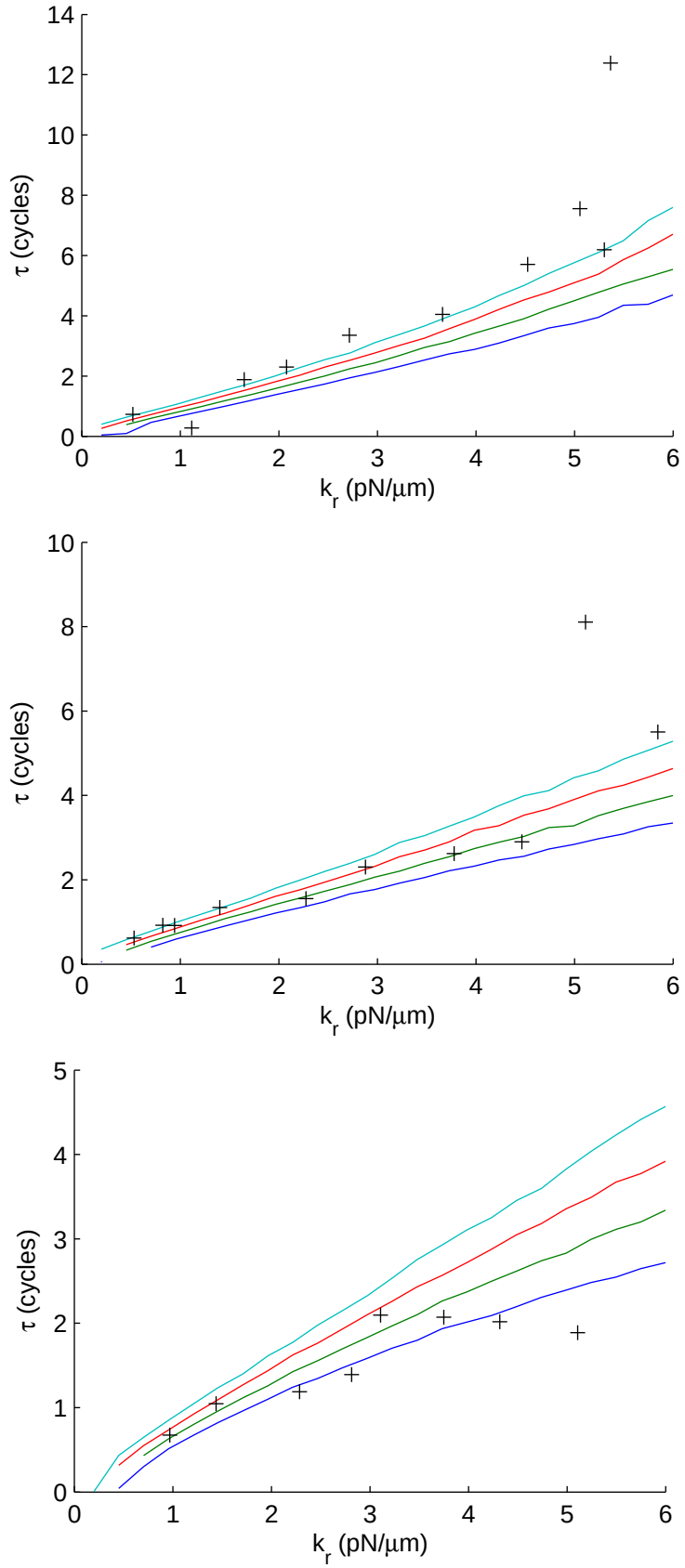

Supplementary Figure S7: Strength of synchronization. Parameter k_r is varied for several values of A_2: 0, 0.4 and 0.7 (from top to bottom). Markers are experimental points and the solid lines are simulations with a delay of 5, 10, 15 and 20 ms (from blue to cyan).

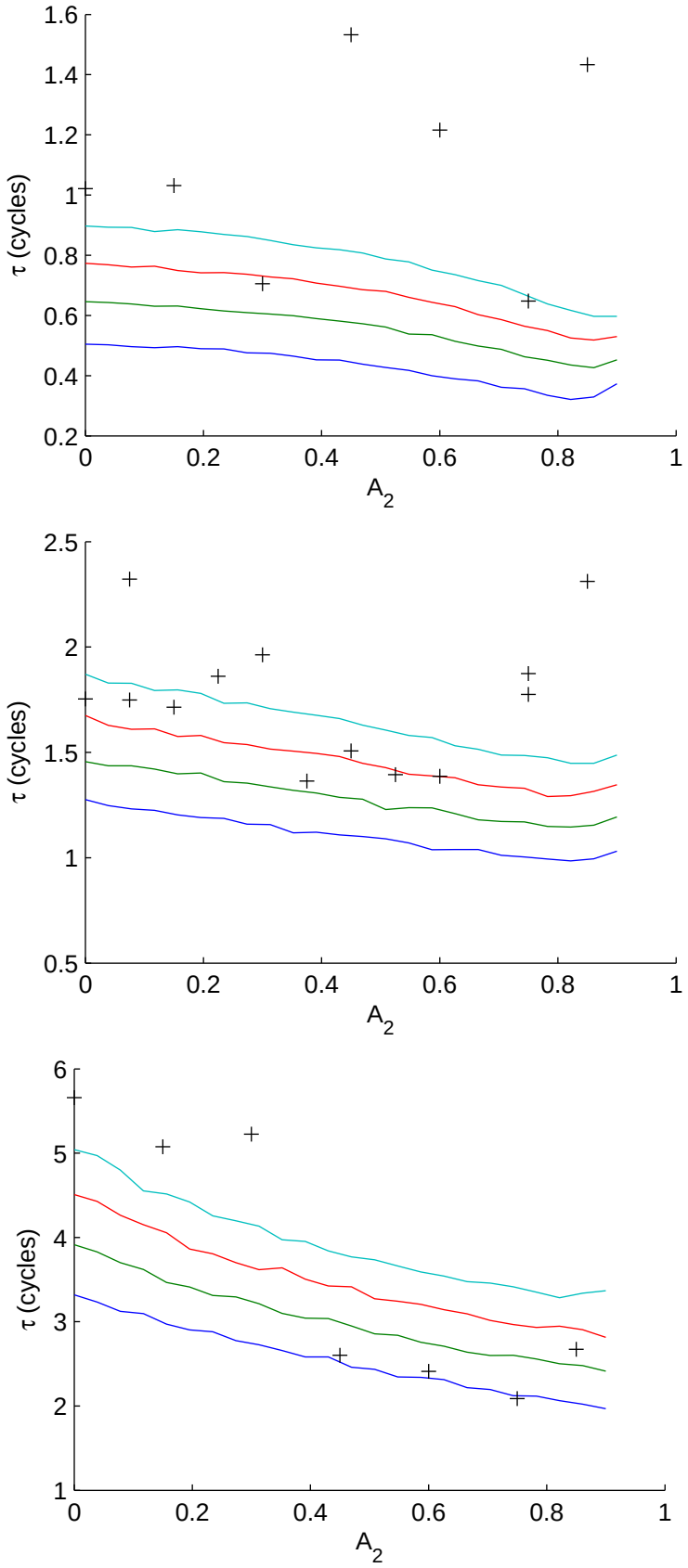

Supplementary Figure S8: Relaxation time of the phase difference between the two oscillators. Parameter A_2 is varied for several values of k_r: 0.762, 1.814 and 4.480 pN/μm (from top to bottom). Markers are experimental points and the solid lines are simulations with a delay of 5, 10, 15 and 20 ms (from blue to cyan).

1.7 Viscosity and local heating

The laser beam of the tweezers delivers a power of a few hundreds of milliwatts at the objective. When entering the sample, the beam heats the fluid. This can create convection and affect the local viscosity.

Viscosity is chosen by preparing water/glycerol solutions. Solutions of 49.6 % in mass glycerol are made, which corresponds to an expected viscosity of 6 mPa·s at 25°C. We measured the viscosity by looking at the autocorrelation of the position of a particle in a static harmonic trap and found 5.5 mPa·s (average over x and y and over several trapping constants; points are spread with a ~ 0.3 mPa·s standard deviation).

The measured value is slightly lower than the expected value. This could be due to heating of the fluid from the laser beam (about 5 °C, measured using the ratio of two fluorescent dyes), or to the uncertainty in the beads' radii (10 % according to manufacturer).

1.8 Wall interaction

The sample is made of a (very) dilute colloids solution sealed between a microscope slide and a cover slip. The film of fluid between the slides is about 150 μm thick. The two rotors are created at a height of 50 μm from the coverslip. Wall effects are not included in the simulations and the theory and they could explain the difference observed in the experiments.

We estimate the hydrodynamic coupling term by calculating the x, x and y, y components of the mobility matrix by using different tensors. Coupling is defined by

$$c^{\alpha,\beta} = \frac{\mu_{1,1}^{\alpha,\beta}}{\mu_{1,2}^{\alpha,\beta}} \tag{S4}$$

with $\alpha, \beta \in \{\text{'}x\text{'}, \text{'}y\text{'}\}$.

To estimate the coupling in the presence of the wall, we use the Blake tensor μ^B corrected for finite-sized particles (as used in [2]). In our geometry, the coupling depends on the distance between the beads d, the distance h between the oscillators and the wall, and the size of the particles a. This geometry reduces the components of the Blake mobility matrix to:

$$\begin{aligned}\mu_{1,2}^{B,x,x} = \frac{1}{12\pi\eta d^3\bar{r}^9}\Big(&- 4a^4d^3\left(d^4 - 27d^2h^2 + 16h^4\right) \\ &- 3d^3\bar{r}^4\left(d^4 + 4h^2d^2 + 12h^4\right) \\ &+ 3d^2\bar{r}^5\left(d^4 + 8h^2d^2 + 16h^4\right) \\ &- 2a^2d^3\bar{r}^2\left(-d^4 + 22d^2h^2 - 16h^2\right) \\ &- 8a^2\bar{r}^3h^2\left(3d^4 + 12d^2h^2 + 16h^4\right)\Big)\end{aligned} \tag{S5}$$

$$\begin{aligned}\mu_{1,2}^{B,y,y} = \frac{1}{24\pi\eta d^3\bar{r}^7}\Big(&3\bar{r}^4d^2\left(-d^3 - 6dh^2 + \bar{r}^3\right) \\ &+ 2a^2\bar{r}^2\left(-d^5 + 8d^3h^2 + d^4\bar{r} + 8d^2h^2\bar{r} + 16h^4\bar{r}\right) \\ &+ 2a^4d^3\left(d^2 - 16h^2\right)\Big)\end{aligned} \tag{S6}$$

$$\mu_{1,1}^{B,x,x} = \mu_{1,1}^{B,y,y} = \frac{1}{6\pi\eta a}\left(1 - \frac{9}{16}\frac{a}{h} + \frac{1}{8}\left(\frac{a}{h}\right)^3 - \frac{1}{16}\left(\frac{a}{h}\right)^5\right) \tag{S7}$$

where

$$\bar{r} = \sqrt{d^2 + (2h)^2}. \tag{S8}$$

The couplings from the Oseen and Blake tensors are compared in Fig. S9 for various heights. At $h = 50$ μm, the wall reduces the coupling by 15 % in the x, x direction and 30 % in the y, y direction, hence increasing the relaxation time.

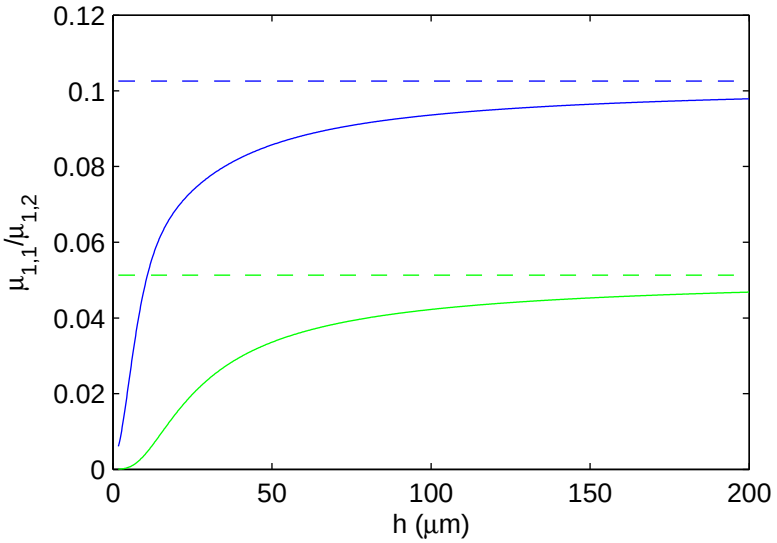

Supplementary Figure S9: Hydrodynamic coupling terms in the x, x (blue) and y, y (green) directions using the Oseen (dashed lines) and Blake (plain lines) tensors. The Blake tensor includes here a correction for the particles' radii. The rotors in the experiments are made at 50 μm from the glass slide, and from this analysis one expects a correction to the Oseen hydrodynamic coupling of about 20%.

1.9 Asymmetries in the setup

The experimental setup might introduce some asymmetries not included in the simulations. Especially, aberrations of the laser beam and calibration of the centre of a trap relative to the video image distort the expected force profile. Therefore, the force profile (see section 1.1) is calibrated from experimental data. However, other variables could suffer from asymmetries and change the strength of synchronization.

Fig. S10 shows experiments with the same parameters, except the orientation of the rotors relative to the rest of the setup. The angle of the line between the centres of the two oscillators is changed between 0 and 90°. The force profiles and the radial stiffness (not shown here) remain constants and the relaxation time fluctuates slightly, but is still much higher than expected for all angles.

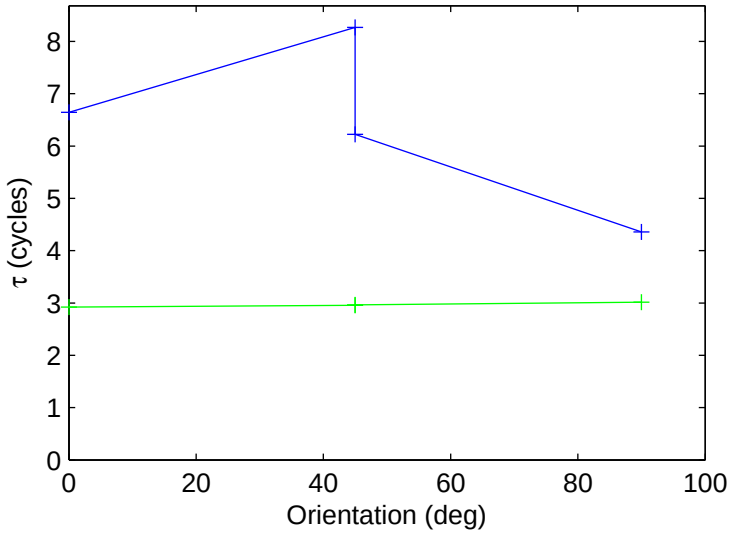

Supplementary Figure S10: Relaxation time of the phase difference in a two rotors experiments. Experiments in blue, theory in green. The orientation of the system is varied by changing the angle between 0 and 90°. It can be interesting to appreciate how optical trap potentials are not "perfectly" rotationally symmetric, but nothing here indicates that this imperfection has any relation to the weaker than expected hydrodynamic coupling.

1.10 Conclusion

From all these checks, it emerges that several points can lead to significantly longer relaxation times in the experiments. The three most significant are:

- The experimental delay between the decision to move a trap and the actual change of the trap position,
- The wall interactions that tend to reduce the hydrodynamic coupling,
- The residual experimental detuning between the intrinsic periods of the two oscillators.

Each of these three are possible reasons behind the increase of the relaxation time in experiments compared to theory; we have estimated that each one can account for a factor which is smaller, but of the order of, the discrepancy that we observe. It is therefore very likely that a combination of these factors is present, leading to the overall weaker synchronization in the experiments compared to the simulations and theory. It is also possible that the experimental measurement of the radial stiffness k_r is not exactly in the same range that is relevant for the two rotor experiments.

A fully quantitative comparison of the experiments against numerical simulations would thus require to include several new parameters in the simulation. We have used instead a different — and simpler — approach to compare experiments and simulations/theory in the main text, by introducing an empirical corrective multiplicative coefficient between the experimentally measured stiffness and the k_r parameter input in the simulations and the theoretical formula. A single multiplicative correction factor is sufficient to provide agreement with all the experimental data.

2 Derivation of the coupling strength Γ

We use all the symbols as defined in the main text, except that we rename the radii as R to avoid confusion with position vectors, and Γ is of opposite sign. This derivation closely follows [3], but with the

radial force only depending on the radial position, hence introducing the Lenz and Golestanian models in a more decoupled way, and possibly matching better the experiments with a laser intensity spread landscape along the R direction.

Let the pair of rotors (indexed $i = 1, 2$) lie in the x-y plane. The spheres are of radius a and have polar coordinates (R_i, ϕ_i), taken relative to an orbit centre $\mathbf{r}_{i0}$. The angular coordinate ϕ_i (or phase) is measured counter-clockwise from the positive x-direction. We also define the unit vectors $\mathbf{e}_{\phi i} = (-\sin\phi_i, \cos\phi_i, 0)$ and $\mathbf{e}_{Ri} = (\cos\phi_i, \sin\phi_i, 0)$ in the angular and radial directions respectively. The position of sphere i is then given by $\mathbf{r}_i = \mathbf{r}_{i0} + R_i\mathbf{e}_{Ri}$ and its velocity by $\dot{\mathbf{r}}_i = R_i\dot{\phi}_i\mathbf{e}_{\phi i} + \dot{R}_i\mathbf{e}_{Ri}$. The orbit centres are positioned such that $\mathbf{r}_{20} - \mathbf{r}_{10} = d\mathbf{e}_x$ where $\mathbf{e}_x$ is a unit vector in the x-direction. The force applied to sphere i is $\mathbf{F}_i = F(\phi_i)\mathbf{e}_{\phi i} - k_r(R_i - R_0)\mathbf{e}_{Ri}$, where $F(\phi_i)$ is the angular driving force, k_r is the radial stiffness and R_0 is the equilibrium radius.

In the following, we will assume that $a \ll d$ and $R_i \ll d$. We will discard terms of order $(a/d)^2$, $(R_i/d)^2$ and aR_i/d^2. We will also assume that there is no substrate. Under these assumptions, the Oseen tensor is a suitable approximation for the mobility:

$$\boldsymbol{H}_{ii} = \gamma^{-1}\left[\mathbf{I} + O(a/d)^4\right], \tag{S9}$$

$$\boldsymbol{H}_{ij} = \gamma^{-1}\left[\frac{3a}{4r_{ij}}\left(\mathbf{I} + \hat{\mathbf{r}}_{ij}\otimes\hat{\mathbf{r}}_{ij}\right) + O(a/d)^3\right], \quad j \neq i, \tag{S10}$$

$$\approx \gamma^{-1}\left[\frac{3a}{4d}\left(\mathbf{I} + \mathbf{e}_x\otimes\mathbf{e}_x\right) + O(aR/d^2)\right], \quad j \neq i, \tag{S11}$$

where $r_{ij} = |\mathbf{r}_j - \mathbf{r}_i| \approx d(1 + O(R/d))$ and $\hat{\mathbf{r}}_{ij} = (\mathbf{r}_j - \mathbf{r}_i)/r_{ij} \approx \mathbf{e}_x + O(R/d)$. The drag coefficient $\gamma = 6\pi\eta a$, where η is viscosity.

Following from Eq. (1) from the main text, the radial and angular components of the force balance equation are

$$\dot{R}_i = \gamma^{-1}\left(-k_r(R_i - R_0) + \left(\frac{3a}{4d}(\mathbf{I} + \mathbf{e}_x\otimes\mathbf{e}_x)\mathbf{F}_j\right)\cdot\mathbf{e}_{Ri}\right), \tag{S12}$$

$$R_i\dot{\phi}_i = \gamma^{-1}\left(F(\phi_i) + \left(\frac{3a}{4d}(\mathbf{I} + \mathbf{e}_x\otimes\mathbf{e}_x)\mathbf{F}_j\right)\cdot\mathbf{e}_{\phi i}\right). \tag{S13}$$

The flow from sphere j varies according to a timescale $\approx \dot{\phi}$. For a given flow there is a stable value of R_i, and solving Eq. S12 tells us that the decay to this stable value follows $R_i(t) \propto \exp(-k_r t/\gamma)$. If we assume that the radial timescale is much faster than the angular one (i.e. $k_r/\gamma \gg \dot{\phi}$), we can imagine that R_i adjusts to the changing flow instantaneously. In this case, $\dot{R}_i = 0$. Following from this, it can be seen that the radial restoring force $k_r(R_i - R_0)$ is of order a/d. Also, $F(\phi_i) = \gamma R_i\dot{\phi}_i + O(a/d)$. Therefore $\mathbf{F}_j$ in Eqs. S12 and S13 can be expanded as $\gamma R_j\dot{\phi}_j\mathbf{e}_{\phi j} + O(a/d)$. After some rearrangement,

$$R_i = R_0 + \frac{3a\gamma R_j\dot{\phi}_j}{8dk_r}\left(3\sin(\phi_i - \phi_j) - \sin(\phi_i + \phi_j)\right), \tag{S14}$$

$$\dot{\phi}_i = \frac{F(\phi_i)}{\gamma R_i} + \frac{3aR_j\dot{\phi}_j}{8dR_i}\left(3\cos(\phi_i - \phi_j) - \cos(\phi_i + \phi_j)\right). \tag{S15}$$

Substituting Eq. S14 into S15 and discarding higher order terms in a/d gives

$$\dot{\phi}_i = \frac{F(\phi_i)}{\gamma R_0} - \frac{3aF(\phi_i)F(\phi_j)}{8\gamma R_0^2 dk_r}(3\sin(\phi_i - \phi_j) - \sin(\phi_i + \phi_j)) + \frac{3aF(\phi_j)}{8\gamma R_0 d}(3\cos(\phi_i - \phi_j) - \cos(\phi_i + \phi_j)). \tag{S16}$$

The rate of change in phase difference between rotor 1 and 2 is therefore

$$\dot{\phi}_1 - \dot{\phi}_2 = \frac{F(\phi_1) - F(\phi_2)}{\gamma R_0} - \frac{9aF(\phi_1)F(\phi_2)}{4\gamma R_0^2 dk_r}\sin(\phi_1 - \phi_2) + \frac{3a(F(\phi_2) - F(\phi_1))}{8\gamma R_0 d}[3\cos(\phi_1 - \phi_2) - \cos(\phi_1 + \phi_2)]. \tag{S17}$$

Setting $\phi_1 = \phi + \delta$ and $\phi_2 = \phi$ and linearizing Eq. S17 about $\delta = 0$ gives the rate at which a small phase difference decays,

$$\frac{\dot{\delta}}{\delta} = \frac{F'(\phi)}{\gamma R_0} - \frac{9aF^2(\phi)}{4\gamma R_0^2 dk_r} - \frac{3aF'(\phi)}{8\gamma R_0 d}(3 - \cos 2\phi), \tag{S18}$$

where $F'(\phi)$ is the derivative of $F(\phi)$ with respect to ϕ. The average decay rate over the cycle is found by evaluating the integral

$$\Gamma = \int_0^{2\pi} \frac{\dot{\delta}}{\delta\dot{\phi}} d\phi, \tag{S19}$$

where Γ is in units of cycles^{-1} and $\dot{\phi}$ is given by Eq. S16, using $\phi_1 = \phi_2 = \phi$ and $F(\phi_1) = F(\phi_2) = F(\phi)$. Substituting this and Eq. S18 into the integral and removing the higher order terms from its Taylor expansion gives

$$\Gamma = \int_0^{2\pi} \left(\frac{F'(\phi)}{F(\phi)} - \frac{3a}{4d}\frac{F'(\phi)}{F(\phi)}(3 - \cos 2\phi) - \frac{9aF(\phi)}{4dk_rR_0} - \frac{3aF'(\phi)}{8dk_rR_0}\sin 2\phi \right) d\phi. \tag{S20}$$

To investigate the effects of different force profiles a Fourier representation is used,

$$F(\phi) = F_0 \left[1 + \sum_{n=1}^{\infty} A_n \sin(n\phi + B_n) \right]. \tag{S21}$$

Substituting this into Eq. S20 gives

$$\Gamma = \frac{3\pi a}{2d} \left(A_2 \cos B_2 - \frac{3F_0}{k_rR_0} + \frac{F_0 A_2 \sin B_2}{2k_rR_0} + O(A_n^2) \right). \tag{S22}$$

Therefore, to first order in A_n, only A_2 affects the decay rate (the other Fourier components are included at higher orders, however). For stable synchronization, Γ should be negative. Since the third term in Eq. S22 is small (due to the earlier assumption that $k_r/\gamma \gg \dot{\phi}$), a suitable choice of coefficients is $0 \leq A_2 < 1$ and $B_2 = \pi$, giving the force profile $F(\phi) = F_0(1 - A_2 \sin 2\phi)$. The decay rate for this force profile, including all orders of A_2, is

$$\Gamma = \frac{3\pi a}{2d} \left(\frac{2}{A_2} \left(\sqrt{1 - A_2^2} - 1 \right) - \frac{3F_0}{k_rR_0} \right). \tag{S23}$$

How does this compare to previously published results? Niedermayer *et al.* [4] studied a pair of rotors with a uniform force profile. They found the instantaneous decay rate to be $\dot{\delta}/\delta = -9a\gamma\omega^2/4dk_r$, where ω is the angular speed of a rotor in isolation. In our system, ω varies with phase. Using $\omega(\phi) = F_0(1 - A_2 \sin 2\phi)/\gamma R_0$ and Eq. S19, the cycle-averaged decay rate is $\Gamma_L = -9\pi a F_0/2dk_rR_0$, which is equal to the second term in Eq. S23. Note that, in the main text, Γ_L is calculated by assuming that ω is constant, and scaling it according to the time period of the force-varied rotor. The sign is also reversed according to the convention used there. This leads to a different expression for Γ_L but the surface plotted in Fig. 3 is very similar.

Meanwhile, Uchida and Golestanian [3] studied rotors with non-uniform force profiles but no radial flexibility ($k_r = \infty$). For the force profile $F(\phi) = F_0(1 - A_2 \sin 2\phi)$, their work implies that the decay rate is $\Gamma_G = 3\pi a(\sqrt{1 - A_2^2} - 1)/A_2 d$. This is equal to the first term of Eq. S23. Therefore, when radial flexibility and a non-uniform force profile are combined, their effects are superposed; we have $\Gamma = \Gamma_L + \Gamma_G$. In the main text, Γ_G is written to first order in A_2 and the sign is reversed.

We note that Uchida and Golestanian have also considered force variation with radial flexibility. However, they model a slightly different system where the laser focus is constrained to a fixed trajectory.

References

[1] J. K. G. Dhont, *An Introduction to Dynamics of Colloids*. Elsevier Science, Jun. 1996.

[2] M. Vilfan, A. Potočnik, B. Kavčič, N. Osterman, I. Poberaj, A. Vilfan, and D. Babic, "Self-assembled artificial cilia," *Proc. Natl. Acad. Sci.*, vol. 107, pp. 1844–1847, 2010.

[3] N. Uchida and R. Golestanian, "Hydrodynamic synchronization between objects with cyclic rigid trajectories," *The European Physical Journal E*, vol. 35, pp. 1–14, 2012.

[4] T. Niedermayer, B. Eckhardt, and P. Lenz, "Synchronization, phase locking, and metachronal wave formation in ciliary chains," *Chaos*, vol. 18, p. 037128, 2008.